

What dictates soft clay-like Lithium superionic conductor formation from rigid-salts mixture

Sunny Gupta^{1,2}, Xiaochen Yang^{1,2}, Gerbrand Ceder^{1,2*}

¹Department of Materials Science & Engineering, UC Berkeley, Berkeley, CA, 94720, USA

²Materials Sciences Division, Lawrence Berkeley National Laboratory, Berkeley, CA, 94720, USA

Abstract

Soft clay-like Li-superionic conductors have been recently synthesized by mixing rigid-salts. Through computational and experimental analysis, we clarify how a soft clay-like material can be created from a mixture of rigid-salts. Using molecular dynamics simulations with a deep learning-based interatomic potential energy model, we uncover the microscopic features responsible for soft clay-formation from ionic solid mixtures. We find that salt mixtures capable of forming molecular solid units on anion exchange, along with the slow kinetics of such reactions, are key to soft-clay formation. Molecular solid units serve as sites for shear transformation zones, and their inherent softness enables plasticity at low stress. Extended X-ray absorption fine structure spectroscopy confirms the formation of molecular solid units. A general strategy for creating soft clay-like materials from ionic solid mixtures is formulated.

Introduction

Mechanically soft materials that can be easily deformed by hand are ubiquitous in nature, such as natural soft-clay¹, dough², gel³, etc. Such materials usually consist of hard and soft components^{1,3,4}, where the former gives rigidity, while the latter gives soft rheological behavior. For example, in natural soft-clays, hard components are layered-minerals such as pyrophyllite¹, while the soft component is water. Soft materials are highly sought after in various applications such as in flexible electronics⁵, pharmaceuticals for drug delivery⁴, and all-solid state batteries to improve fabrication, and interfacial kinetics⁶⁻⁸.

Recently, such soft clay-like materials were introduced into the energy storage field as potential fast Li-ion conductors. Somewhat surprisingly, a soft clay-like material was synthesized by ball milling two rigid salts, LiCl and GaF₃, at room temperature (RT) without water.^{9,10} The resulting amorphous solid had high RT Li-ion conductivity of ~4 mS/cm, which is comparable to that of liquid organic electrolytes. Pliable solid-state ionic conductors are of particular interest as they have the potential to facilitate the fabrication of solid-state batteries and accommodate the swelling of active cathode materials¹¹. The fact that a soft material can be created by merely mixing two rigid ionic solids contradicts conventional thinking. Understanding the physical mechanism behind mechanical softness in such materials and identifying the general criteria for soft-clay formation from mixtures of ionic solids could help to establish design principles for creating innovative soft materials. Combining the exotic properties that can be achieved in ionic

materials, such as magnetism^{12,13}, polaronic optical absorption¹⁴, color centers host¹⁵, magneto-optical response¹⁶, etc., and the novel concept of creating mechanically soft systems from mixtures of ionic solids has far reaching implications.

This study presents a combined computational and experimental analysis of the microscopic mechanism governing soft-clay formation upon mixing two rigid salts, GaF₃ and LiCl. By training a deep learning-based interatomic potential energy (PE) model we were able to explore the mechanical behavior of an amorphous structure with ~10k atoms using molecular dynamics (MD) simulations. The results reveal that the formation of molecular solid-like (MS) units from the chemical reaction between the hard solids, is responsible for the material's mechanical softness. These units serve as sites for shear transformation zones and are inherently soft, enabling plasticity at low stress. Extended X-ray absorption fine structure (EXAFS) of the synthesized soft clay-like material confirmed the formation of these molecular units. This study provides a detailed understanding of the microscopic mechanism of soft-clay formation from rigid ionic solid mixtures and proposes criteria and design strategies for realizing other mechanically soft materials.

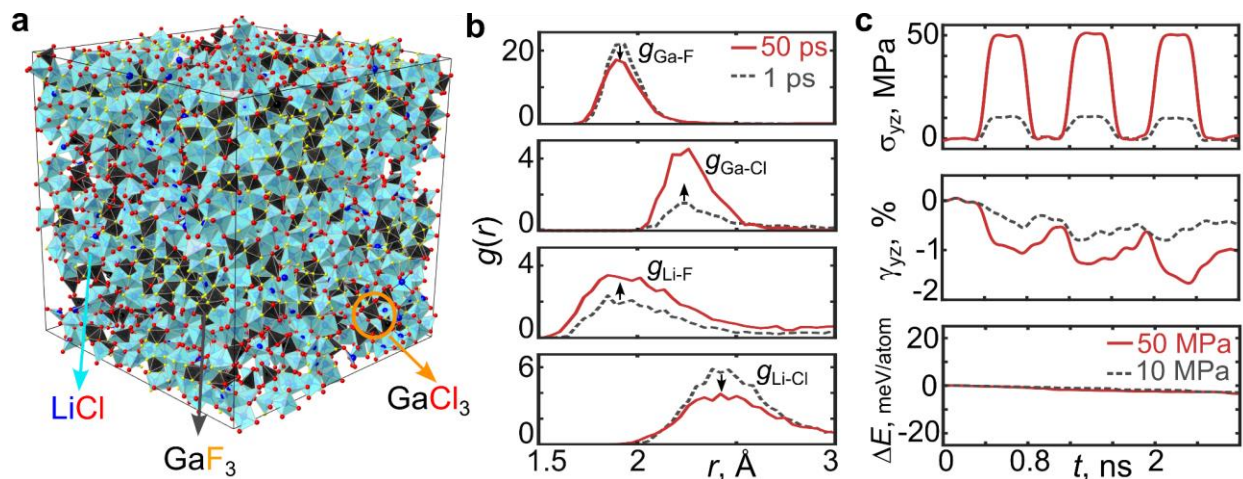


Fig. 1. (a) An amorphous Ga-F-Li-Cl structure constructed for computational modeling, containing domains of LiCl, GaF₃, and GaCl₃-like molecules formed during the high temperature MD simulations. (b) The element-wise radial pair distribution function $g(r)$ plotted at $t = 1$ ps and $t = 50$ ps of the MD simulation at $T = 900$ K. (c) The applied external shear stress σ_{yz} , accumulated shear strain γ_{yz} , and total potential energy change ΔE of the amorphous structure as a function of time in the MD simulation at $T = 300$ K. The external shear stress ranged from 10 to 50 MPa. The accumulated shear strain after three cycles is non-negligible ($\gamma_{yz} \neq 0$), signifying permanent deformation.

Results

LiCl and GaF₃, two rigid salts with melting points 878 K and 1070 K, respectively, were recently found⁹ to form a soft clay-like amorphous solid with a glass transition at $T_g \sim -60$ °C, when ball milled in a molar ratio $x\text{LiCl}:\text{GaF}_3$ ($2 \leq x \leq 4$) for 18 hours at RT (a powder state remained for $x < 2$). To explore the reaction mechanism and mechanical behavior, a deep learning-based interatomic PE model was trained for the Ga-F-Li-Cl chemical system using DeepMD^{17,18} (details in Supplemental material SM-1,2). Training was performed using the atomic forces and energies of ab initio molecular dynamics (AIMD) trajectories of 13 stable crystalline phases in the Ga-F-Li-Cl quaternary chemical space, and 3 slab-like structures of LiCl|GaF₃ (where multilayer slabs of

[001] LiCl and [001] GaF₃ having 3 different thicknesses are interfaced “[|]” (see Fig. S1 and Table SM-1 for the full list of structures). The atomic configurations were obtained by melting and quenching each structure using AIMD simulations. In total, >700k AIMD frames were generated, from which 250k atomic configurations were randomly chosen for training. Our trained model was validated on a subset of training structures, and the RMSE error in energy and forces were <1 meV/atom and <70 meV/Å² after training (Fig. S2). The trained model was also tested on atomic forces and energies of several additional structural configurations (not included in the training and validation set), and benchmarked against their bulk modulus calculated with density functional theory (DFT), and tensile stress-strain response and Li-ion conductivity calculated with DFT-AIMD, and showed good agreement with actual DFT values (see Table SM-2, Fig. S3, S4).

In recent experiments^{9,10}, the amorphous clay-like solid obtained from ball-milled LiCl and GaF₃ was found to contain domains of unreacted parent constituents distributed randomly within the amorphous matrix. To emulate conditions observed in experiments, where LiCl and GaF₃ particles come into contact and react during ball-milling, a specific procedure was designated to create large supercells with domains of each constituent (LiCl and GaF₃). The procedure involved firstly creating a slab-like geometry of LiCl|GaF₃, where a multilayer slab of [001] LiCl and [001] GaF₃ was interfaced in a LiCl:GaF₃ molar ratio of 2. This slab-like structure was subjected to an AIMD simulation under the NVT ensemble for $t = 5$ ps at $T = 800$ K to equilibrate the interface, and then relaxed at $T = 0$ K to a local energy minimum. The resulting structure, as shown in Fig. S5a, was then periodically repeated along the two directions perpendicular to the interface, and a ~2.5 nm cubic “particle” was cut out from it. Eight of these identical ~2.5 nm aperiodic particles, adding up to ~10k atoms, were arranged in a larger cell of size ~5.4 nm (Fig. S5b). To achieve many distinct interfacial environments, each of the ~2.5 nm particles was rotated 90° with respect to their neighbors, such that the axis normal to the interface between LiCl and GaF₃ in each particle did not align in the same direction as that of the neighboring particles (additional details in SM-3 and Fig. S5). Relaxing the cell in LAMMPS¹⁹ using the trained deep-learning based PE model at $T = 0$ K, densified the system by removing the vacuum between each ~2.5 nm cube of material. This relaxed structure with ~10k atoms was subjected to a high-temperature classical MD simulation (hereafter, unless specified, all MD simulations were done with LAMMPS¹⁹ using the trained deep learning-based PE model) under the NVT ensemble for $t = 50$ ps at $T = 900$ K to allow mixing of the atoms. To obtain a representative structure in which domains of reactant materials are visible, an atomic configuration at $t = 50$ ps was selected and this configuration was relaxed in LAMMPS at $T = 0$ K to a local energy minimum (this procedure is analogous to the commonly used melt and quench techniques^{20,21} to create amorphous structures). The relaxed structure was further equilibrated in an MD simulation under the NPT ensemble for a duration of 2 ns at $T = 300$ K and zero external stress, until there was no further change in density, lattice constant, angles, or total potential energy. The resulting amorphous structure is shown in Fig. 1a and exhibits chemical heterogeneity with domains of unreacted LiCl and GaF₃, as well as the formation of GaCl₃-like units. The specific volume of the structure was computed at different temperatures, and a glass-like transition was observed at $T_g \sim -58$ °C (Fig. S7), in good agreement with experiments⁹. Fig. 1b shows the element-wise radial pair distribution function $g(r)$ before and after the high temperature ($T = 900$ K) MD simulation of $t = 50$ ps. The Ga-F and Li-Cl peak decrease, while the Ga-Cl and Li-F peak increase, indicating that anion exchange occurs when the two salts are mixed. This anion exchange is consistent with thermodynamic driving force.

Considering all possible phases that can form when LiCl and GaF₃ react, using entries from the Materials Project database²², the thermodynamic driving force is found to be maximum (reaction energy is most negative) for the anion exchange reaction $3\text{LiCl} + 2\text{GaF}_3 \rightarrow 1\text{Li}_3\text{GaF}_6 + 1\text{GaCl}_3$, $E_{\text{rxn.}} = -87 \text{ meV/atom}$ (Fig. S6).

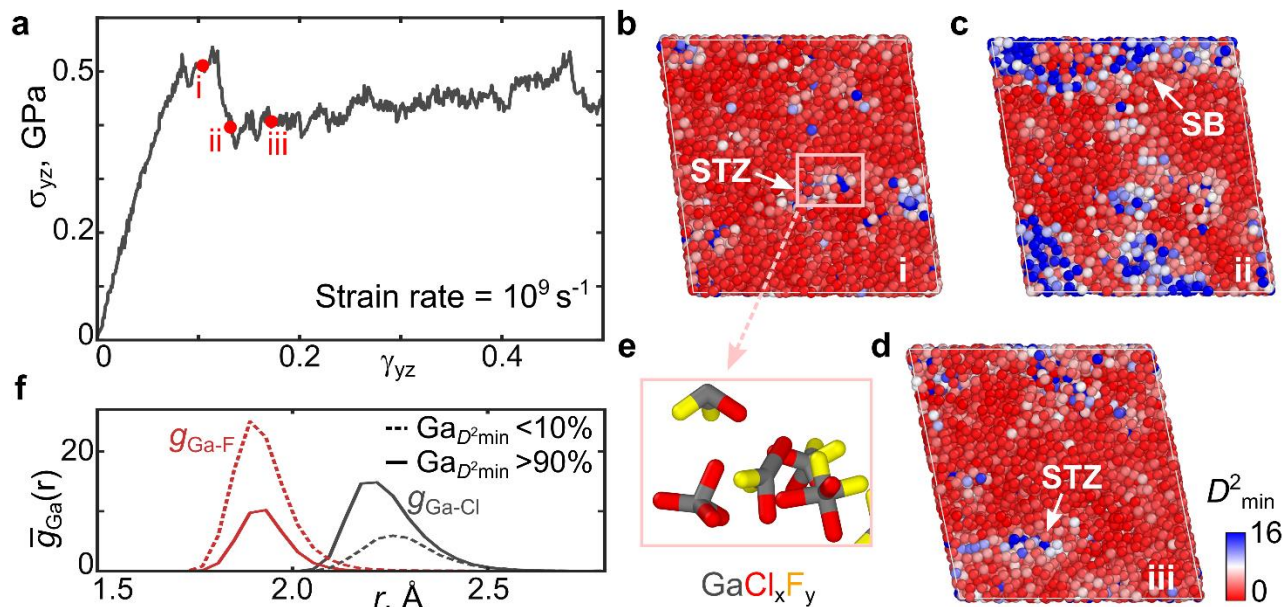


Fig. 2. (a) Shear stress (σ_{yz}) strain (γ_{yz}) response of the amorphous structure at $T = 300 \text{ K}$ at a constant applied shear strain rate of 10^9 s^{-1} . (b - d) Shows snapshots of the material at different strain values i - iii in (a). The color (red-low and blue-high) represents the value of non-affine displacement D^2_{min} , at an interval of $\Delta\gamma_{yz} = 0.01$. In (b, i) the shear transformation zone (STZ) formed is indicated by an arrow and marked by a pink square. In (c, ii) the arrow points to shear bands (SB). (e) Shows the atoms that are part of the STZ in the pink square in (b, i) and have large D^2_{min} values. These are mostly GaCl₃-like and Cl-rich GaCl_xF_y complexes. (f) The Ga-Cl and Ga-F pair distribution function $g(r)$ of Ga-atoms with largest ($D^2_{\text{min}} > 90\%$ of maximum) and smallest ($D^2_{\text{min}} < 10\%$ of maximum) non-affine displacement values. The $g(r)$ values were averaged over the strain interval $\gamma_{yz} = 0.09 - 0.14$.

To determine whether our amorphous structure (Fig. 1a) exhibits soft mechanical behavior similar to that observed in experiments, we simulated the response of the system in a stress-controlled MD simulation under an NPT ensemble at 300 K. The simulation involved subjecting the system to an external shear stress, specifically setting the yz -component σ_{yz} to either 10 MPa or 50 MPa, while keeping all the other external stress components at zero. The shear stress was applied for 400 ps and then released for 400 ps, and this stress pulse was repeated three times. Fig. 1c shows the resulting shear strain γ_{yz} , and total potential energy ΔE . The external stresses' yz -component was arbitrarily chosen and was found not to influence the results (see Fig. S10 for results when xz -component of external stress was applied and other components were kept at zero). The accumulated shear strain after three loading cycles is non-negligible, and the structure exhibits permanent deformation and plastic behavior, even at low $\sigma_{yz} = 10 \text{ MPa}$. This shows that the amorphous structure is mechanically soft, similar to what is observed in experiments. The change in potential energy after deformation is small $< 3 \text{ meV/atom}$. The small change in potential

energy upon application of stress cycles is expected in glasses, which typically have a fractal-like PE surface^{23,24}, and indicates that the amorphous structure (Fig. 1a) is in a meta-basin. A glassy material can hop between near-degenerate sub-basins within a meta-basin and achieve plasticity even at low stresses²⁴. Analysis at even lower shear stresses $\sigma_{yz} < 10$ MPa, could not be performed due to stress fluctuations of that order in the simulations.

To further investigate the microscopic features responsible for the material's soft plastic response, we performed another MD simulation at a constant strain rate and $T = 300$ K (additional details in SM-1). Such strain-controlled MD simulations are commonly employed^{24,25} to identify the microscopic plastic events, as they enable the separation of the elastic and plastic regions based on strain magnitudes. Fig. 2a shows the shear stress-strain response of the structure (Fig. 1a) at an applied shear strain rate of 10^9 s⁻¹ on the yz plane. While the obtained yield stress under this very high strain rate is ~ 0.5 GPa (Fig. 2a), the stress is expected to be much lower under a lower strain rate^{24,25}. Lower strain rates, as used in experiments are not directly accessible in molecular dynamics, and methods such as metadynamics²⁴ would have to be used. However, our results using a constant stress (Fig. 1c) demonstrate that the material is indeed soft. A non-elastic plastic response is evident at $\gamma_{yz} > 0.05$ in Fig. 2a. Deviation from the elastic response in amorphous materials can be quantified by the non-affine displacements (D_{\min}^2)^{24,26}. A method previously²⁶ reported to calculate D_{\min}^2 was used here (see details in SM-6). Fig. 2b-d shows snapshots of the structures at three different (i - iii) γ_{yz} values with the local value of D_{\min}^2 represented by the color legend. In structure i (Fig. 2b), at a low shear strain, the areas with non-zero D_{\min}^2 indicate local plastic deformation, commonly known as Shear Transformation Zones (STZs)^{24,26,27} in amorphous materials. In structure ii (Fig. 2c), where γ_{yz} has increased, these STZs form shear bands²⁴⁻²⁷. Moreover, in structure iii (Fig. 2d), with further increased γ_{yz} , localized STZs similar to those observed in structure i (Fig. 2b) reappear. The MD simulation at a constant strain rate (Fig. 2a-d) reveals that our structure exhibits plastic deformation by forming STZs and shear bands, which are characteristic of plastic deformation in amorphous materials²⁴⁻²⁷.

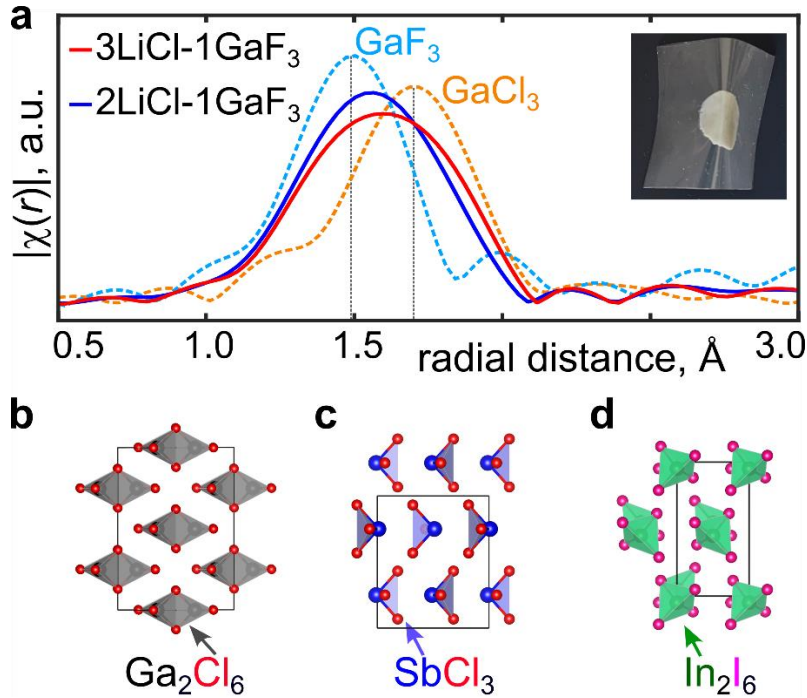


Fig. 3. (a) Ga K-edge EXAFS of different materials, bulk GaF_3 , bulk GaCl_3 , and clay-like $2\text{LiCl}-1\text{GaF}_3$ and $3\text{LiCl}-1\text{GaF}_3$. $|\chi(r)|$, magnitude of Fourier transformed EXAFS. Inset shows an image of synthesized soft clay-like $2\text{LiCl}-1\text{GaF}_3$ bent into a particular shape. (b, c, d) Bulk crystal structure of molecular solids GaCl_3 , SbCl_3 , and InI_3 , respectively.

To understand the local chemical environment of STZs responsible for plastic deformation, we plotted in Fig. 2f the radial distribution function $g(r)$ around Ga atoms with the highest and lowest D^2_{\min} values. The $g(r)$ was averaged over the strain interval $\gamma_{yz} = 0.09 - 0.14$. We found that Ga atoms in the areas involved in plastic deformation have a Cl-rich environment, as evidenced by the lower Ga-F peak for Ga atoms with $D^2_{\min} > 90\%$ of maximum compared to those with D^2_{\min} values $< 10\%$ of maximum (Fig. 2f). Additionally, we visually examined the local structure in STZs and found that it mostly consists of GaCl_3 -like and Cl-rich GaCl_xF_y complexes (Fig. 2e). As illustrated in Fig. 3b bulk GaCl_3 is a molecular solid consisting of Ga_2Cl_6 complexes that are Van der Waals bonded to each other. The weak intermolecular interactions in molecular solids render them intrinsically very soft²⁸. The nature of this weak bonding rationalizes why strain localizes in areas where Ga is mostly coordinated by Cl in our simulations. These findings indicate that the soft plastic behavior in the $2\text{LiCl}-\text{GaF}_3$ structure arises due to the formation of molecular solid-like GaCl_3 -units and Cl-rich GaCl_xF_y complexes during anion exchange. These complexes are activated at low stresses to form STZs, ultimately leading to soft-plastic deformation. Thus, the formation of molecular solid units is the key to the soft clay-like plastic response.

Table 1: Showing different salt combinations (precursors) considered in this study for possible soft-clay formation. The predicted products are based on the maximum thermodynamic driving force with the maximum (most negative) reaction energy (E_{rxn}). Possible molecular solid component that can form is also listed. Additionally, the crystalline phases in the product, formed after ball milling (BM) the precursors in experiments are identified with X-ray diffraction

(XRD) and listed under the column – XRD peak after BM. The rheological behavior of ball-milled products is also tabulated.

Precursors	Predicted products with maximum E_{rxn}	Possible molecular solid component	XRD peak after BM	Rheological behavior
2LiCl + 1GaF ₃ and 3LiCl + 1GaF ₃	Li ₃ GaF ₆ + GaCl ₃	GaCl ₃	LiCl	soft clay-like
3LiCl + 1SbF ₃	LiF + SbCl ₃	SbCl ₃	LiF + SbCl ₃	powder
3LiI + 1InBr ₃	LiBr + InI ₃	InI ₃	LiBr + InI ₃	powder
3LiI + 1GaF ₃	LiF + GaI ₃	GaI ₃	GaI ₃	powder

To validate anion exchange and the formation of molecular units in the 2LiCl-1GaF₃ and 3LiCl-1GaF₃ soft clay-like materials, we prepared samples by mechanochemically mixing (ball milling) LiCl and GaF₃ precursors in the ratio of 2:1 and 3:1, as previously reported⁹ (further experimental details in SM-5). The inset in Fig. 3a shows an image of the resulting soft clay-like material bent into a specific shape. The RT Li-ion conductivity measured using electrochemical impedance spectroscopy was found to be ~2.9 mS/cm (details in SM-5), similar to that reported in ref. [9]. To understand the local atomic chemical environment of Ga atoms in the soft clay-like materials we performed EXAFS²⁹. Fig. 3a compares the Ga-K edge EXAFS of the ball-milled 2LiCl-1GaF₃ and 3LiCl-1GaF₃ with that of bulk GaF₃ and GaCl₃. The Ga EXAFS curves of 2LiCl-1GaF₃ and 3LiCl-1GaF₃ lie between the curves of bulk-GaF₃ and bulk-GaCl₃ indicating contributions from both GaF₃-like as well GaCl₃-like units. This confirms that anion exchange takes place during the ball milling of a LiCl-GaF₃ mixture forming GaCl₃-like molecular units, consistent with the observations in the MD simulations (Fig. 1b). XRD of the soft clay-like materials (Fig. S8e) did not reveal any peaks corresponding to bulk GaCl₃, indicating that no distinct crystalline GaCl₃ phase formed.

To achieve soft clay-like mechanical behavior, it is necessary to have both soft and hard components¹. In our particular case, hard components are provided by unreacted LiCl and GaF₃, while the GaCl₃-like molecular component provides softness. Soft-clay will not form if the soft component is deficient or in excess, analogous to the appropriate ratio³⁰ of water and pyrophyllite-like minerals to form natural soft-clay. This can happen for GaF₃-rich compositions, $x < 2$ in $x\text{LiCl}:\text{GaF}_3$, which have been observed not to form soft-clay^{9,31}. Moreover, if the soft and hard components phase segregates into macroscopic separate phases, then soft clay-like deformation will also not be achieved. Indeed, ball milling the compounds that would constitute the terminal products of anion-exchange, LiF and GaCl₃, does not lead to a soft-clay. This points at the importance of the kinetics of anion exchange, in addition to the mixture having the right ratio of components. Anion exchange must occur but should not be completed, and the products should not separate into macroscopic phases. Hence, to form soft-clay from ionic solids, three criteria

must be met - (i) the combination of salts must have a thermodynamic driving force for anion exchange leading to units that form molecular solids, (ii) the kinetics of the reaction must be slow enough to avoid complete anion exchange and phase separation, and (iii) the ratio of salts must be in an appropriate range, ensuring that neither of the salt components is in much excess.

In an attempt to find other soft-clay-forming mixtures, we searched the Materials Project database²² and identified three other molecular solids, SbCl_3 , InI_3 , and GaI_3 , which can form through anion exchange from rigid solid mixtures $1\text{SbF}_3\text{-}3\text{LiCl}$, $1\text{InBr}_3\text{-}3\text{LiI}$, and $1\text{GaF}_3\text{-}3\text{LiI}$, respectively (SM-4). The crystal structures of SbCl_3 and InI_3 , depicted in Fig. 3c,d, consist of molecular units that are held together through Van der Waals interactions, while GaI_3 has a similar crystal structure as GaCl_3 (Fig. 3b). Table 1 displays the different salt combinations evaluated in this study for possible soft-clay formation. The mixtures were ball milled and characterized by XRD to identify any crystalline phases formed. We find that in the case of $3\text{LiCl}\text{-}1\text{SbF}_3$, $3\text{LiI}\text{-}1\text{InBr}_3$, and $3\text{LiI}\text{-}1\text{GaF}_3$, a powder state remains after ball milling and a soft-clay does not form (hereafter called non-clay). Additionally, in all three non-clay cases, peaks corresponding to crystalline molecular solid phases (SbCl_3 , InI_3 , and GaI_3) were visible in XRD (see Table 1, Fig. S8). In contrast, for $2\text{LiCl}\text{-}1\text{GaF}_3$ and $3\text{LiCl}\text{-}1\text{GaF}_3$, a mechanically soft solid was obtained after ball milling (hereafter called clay). XRD spectra of the $3\text{LiCl}\text{-}1\text{GaF}_3$ (clay) only showed peaks corresponding to LiCl (unreacted precursor), while no peaks corresponding to any crystalline GaCl_3 were visible (see Table 1, Fig. S8). The appearance of peaks corresponding to crystalline molecular solid phases in the XRD of the non-clay systems, signifies that the molecular solid units have separated into macroscopic phases. Moreover, in the non-clay systems $3\text{LiCl}\text{-}1\text{SbF}_3$, and $3\text{LiI}\text{-}1\text{InBr}_3$, XRD peaks corresponding to the anion exchanged products (apart from MS), LiF and LiBr , were also observed, signifying that the anion exchange products have separated into macroscopic phases. These findings reveal that non-clay formation is linked with the separation of anion exchanged products into macroscopic phases, thereby validating the role of kinetics in soft-clay formation. To form a soft-clay, anion exchange must occur, but the products should not phase segregate into macroscopic separate phases. Furthermore, we tracked the XRD peaks of phases formed at different instances of time during ball milling (see Fig. S8d). For a representative non-clay material $3\text{LiI}\text{-}1\text{InBr}_3$, XRD peaks corresponding to LiBr and InI_3 were seen after just 20 minutes of ball milling, indicating a rapid anion exchange and phase separation, while for the soft clay-like $3\text{LiCl}\text{-}1\text{GaF}_3$, no signatures of anion exchange completion or phase separation were seen even after 24 hours of ball milling. This indicates that the inherent chemistry of GaF_3 impedes kinetics of complete anion exchange and phase separation. Additionally, in non-clay systems, strategies to suppress kinetics, such as regulating temperature during ball milling, can be used for soft-clay formation.

Discussion

Our combined computational and experimental study shows that when a rigid salt mixture of $2\text{LiCl}\text{-}1\text{GaF}_3$ mechanochemically reacts, the resulting system mechanically behaves like a soft-clay, as evidenced in both MD simulations (Fig. 1c) and experiments (Fig. 3a inset), consistent with prior studies^{9,31}. We find that during the ball milling reaction, partial anion exchange takes place and GaCl_3 -like molecular solid (MS) units are formed, which is consistent with the thermodynamic driving force (Fig. S6). This process was confirmed both with MD simulations (Fig. 1a,b and Fig. 2b) and EXAFS (Fig. 3a). MD simulations of the shear stress-strain response of the

material (Fig. 2) show that MS-like units serve as sites for shear transformation zones which get activated at low stress and lead to soft-plastic deformation. These findings point to the formation of molecular solid units as a result of the partial anion exchange, as the key to the soft clay-like mechanical response. Our experiments on other ion-exchange solids indicate that careful tuning of the composition and processing is required to obtain the proper soft mechanical response. Some salt mixtures have a thermodynamic driving force (TDF) for anion exchange reaction, but if the anion exchange reaction does not lead to MS formation, soft-clay will not be obtained. This phenomenon was observed in prior studies^{9,31} for salt mixtures such as 1NaCl-1GaF₃, 3LiCl-1InF₃, 6LiCl-1Ga₂O₃, 3LiOH-1GaF₃, 1Li₂O-1GaF₃, 3LiCl-1LaF₃, where soft-clay formation was unsuccessful. Except for the case of 3LiCl-1InF₃, where there is no TDF for anion exchange reaction, in all other cases, the salt mixtures have a TDF for anion exchange reaction, but the anion exchange reaction does not lead to MS formation (see SM-4). In contrast, the 3LiBr-1GaF₃ mixture was found⁹ to exhibit soft clay-like mechanical behavior driven by the favorable reaction energy of an anion exchange between LiBr and GaF₃ to form GaBr₃ (see SM-4), which is a molecular solid and has a similar crystal structure as GaCl₃ (Fig. 3b).

The kinetics of anion exchange is also important for soft-clay formation. If the anion exchanged molecular species phase segregate into distinct macroscopic phases, then the MS-like soft units will not be interfaced between the hard solids, and soft clay-like mechanical response will not occur. This phenomenon is observed in salts mixture 3LiCl-1SbF₃, 3LiI-1InBr₃, and 3LiI-1GaF₃ (Table 1), where the XRD spectra (Fig. S8) of the ball milled products showed peaks corresponding to crystalline molecular solid phases, indicating that the MS units have separated into macroscopic phases. To suppress kinetics of anion exchange, temperature during ball milling can be regulated. It is intuitive that the appropriate ratio of salts in the mixture is also crucial for soft-clay formation; neither of the salt components should be in much excess. Although important, the exact ratio of salts in the mixture to form soft-clay is challenging to predict, a priori.

The mechanism behind mechanical softness in clay-like Li superionic conductors synthesized from a mixture of rigid salts, in this and prior studies^{9,10,31}, bears resemblance to both natural soft-clays,^{1,30,32} and synthetic soft-clays³³⁻³⁵ formed from a blend of hard minerals and soft polymers. The unifying feature responsible for the pliability of all these soft-clays is the presence of soft components within a rigid matrix. In natural soft-clays, a mixture of hard minerals and water, plasticity arises when platelet-like hard minerals slide over each other upon the addition of water,^{30,32} which acts as the soft component. Moreover, synthetic soft-clays composed of hard minerals dispersed in a soft polymer matrix exhibit plasticity through shear banding of the soft polymers, accompanied by momentum transfer to the rigid minerals.^{33,34} Analogously, in soft clay-like Li superionic conductors created from a mixture of rigid salts, we find that plasticity occurs through the formation of shear transformation zones (STZs) and shear bands at the sites of soft MS-like units between the hard solids (Fig. 2). The inherent softness of MS-like units leads to the activation of STZs at low stresses, resulting in a soft clay-like mechanical response. Additionally, in natural and synthetic soft-clays, factors such as the ratio of rigid to soft units, particle size distribution, specific surface area of particles, and temperature also contribute to the plasticity.^{32,33} Although, determining the precise role of these factors can be challenging, we anticipate that they will significantly influence the pliability of clay-like materials synthesized from a mixture of rigid salts.

In summary, we have uncovered the microscopic mechanism of soft-clay formation from the ionic solid mixtures by studying the mechanical behavior of amorphous $2\text{LiCl}-1\text{GaF}_3$ using MD simulations and with a deep learning-based interatomic PE model. We find that the formation of molecular solid-like units as a result of anion exchange is the key to soft clay-like mechanical behavior. MS-like units serve as the sites for STZs which get activated at low stress and lead to soft-plastic deformation. Additionally, to form soft clay-like systems from generic ionic solid mixtures, three criteria must be met - (i) the combination of salts must have a thermodynamic driving force for anion exchange leading to units that form molecular solids, (ii) the kinetics of the reaction must be slow enough to avoid complete anion exchange and phase separation, and (iii) the ratio of salts must be in an appropriate range, ensuring that neither of the salt components is in much excess. These strategies can be applied to discover other soft clay-like systems from ionic solid mixtures. Additionally, exploiting the inherent properties of ionic solids, these approaches can be used to create flexible magnets, electronic conductors, and other pliable superionic (Mg, Ca, etc.) conductors with wide-ranging implications.

The authors acknowledge the ACCESS (formerly XSEDE) supercomputing resources for providing computing facilities.

References

1. Meunier, A. *Clays*. (Springer Science & Business Media, 2005).
2. Frater, R., Hird, F. J. R., Moss, H. J. & Yates, J. R. A Role for Thiol and Disulphide Groups in Determining the Rheological Properties of Dough Made from Wheaten Flour. *Nature* **186**, 451–454 (1960).
3. Ruzicka, B. *et al.* Observation of empty liquids and equilibrium gels in a colloidal clay. *Nat. Mater.* **10**, 56–60 (2011).
4. Li, J. & Mooney, D. J. Designing hydrogels for controlled drug delivery. *Nat. Rev. Mater.* **1**, 1–17 (2016).
5. Lim, H.-R. *et al.* Advanced Soft Materials, Sensor Integrations, and Applications of Wearable Flexible Hybrid Electronics in Healthcare, Energy, and Environment. *Adv. Mater.* **32**, 1901924 (2020).
6. Chen, R., Li, Q., Yu, X., Chen, L. & Li, H. Approaching Practically Accessible Solid-State Batteries: Stability Issues Related to Solid Electrolytes and Interfaces. *Chem. Rev.* **120**, 6820–6877 (2020).
7. Tian, Y. *et al.* Promises and Challenges of Next-Generation “Beyond Li-ion” Batteries for Electric Vehicles and Grid Decarbonization. *Chem. Rev.* **121**, 1623–1669 (2021).
8. Janek, J. & Zeier, W. G. A solid future for battery development. *Nat. Energy* **1**, 1–4 (2016).
9. Jung, S.-K. *et al.* Pliable Lithium Superionic Conductor for All-Solid-State Batteries. *ACS Energy Lett.* **6**, 2006–2015 (2021).
10. Xu, R. *et al.* Room Temperature Halide-Eutectic Solid Electrolytes with Viscous Feature and Ultrahigh Ionic Conductivity. *Adv. Sci.* **9**, 2204633 (2022).
11. Shi, T. *et al.* Characterization of mechanical degradation in an all-solid-state battery cathode. *J. Mater. Chem. A* **8**, 17399–17404 (2020).
12. Moreira, I. de P. R. *et al.* Local character of magnetic coupling in ionic solids. *Phys. Rev. B* **59**, R6593–R6596 (1999).

13. Koshihara, S. *et al.* Ferromagnetic Order Induced by Photogenerated Carriers in Magnetic III-V Semiconductor Heterostructures of (In,Mn)As/GaSb. *Phys. Rev. Lett.* **78**, 4617–4620 (1997).
14. Emin, D. Optical properties of large and small polarons and bipolarons. *Phys. Rev. B* **48**, 13691–13702 (1993).
15. Seitz, F. Color Centers in Alkali Halide Crystals. *Rev. Mod. Phys.* **18**, 384–408 (1946).
16. Casals, B. *et al.* Giant Optical Polarization Rotation Induced by Spin-Orbit Coupling in Polarons. *Phys. Rev. Lett.* **117**, 026401 (2016).
17. Wang, H., Zhang, L., Han, J. & E, W. DeePMD-kit: A deep learning package for many-body potential energy representation and molecular dynamics. *Comput. Phys. Commun.* **228**, 178–184 (2018).
18. Zhang, L., Han, J., Wang, H., Car, R. & E, W. Deep Potential Molecular Dynamics: A Scalable Model with the Accuracy of Quantum Mechanics. *Phys. Rev. Lett.* **120**, 143001 (2018).
19. Thompson, A. P. *et al.* LAMMPS - a flexible simulation tool for particle-based materials modeling at the atomic, meso, and continuum scales. *Comput. Phys. Commun.* **271**, 108171 (2022).
20. Shi, Y. & Falk, M. L. Strain Localization and Percolation of Stable Structure in Amorphous Solids. *Phys. Rev. Lett.* **95**, 095502 (2005).
21. Zhao, X., Ceresoli, D. & Vanderbilt, D. Structural, electronic, and dielectric properties of amorphous ZrO₂ from ab initio molecular dynamics. *Phys. Rev. B* **71**, 085107 (2005).
22. Jain, A. *et al.* Commentary: The Materials Project: A materials genome approach to accelerating materials innovation. *APL Mater.* **1**, 011002 (2013).
23. Charbonneau, P., Kurchan, J., Parisi, G., Urbani, P. & Zamponi, F. Fractal free energy landscapes in structural glasses. *Nat. Commun.* **5**, 3725 (2014).
24. Cao, P., Short, M. P. & Yip, S. Potential energy landscape activations governing plastic flows in glass rheology. *Proc. Natl. Acad. Sci.* **116**, 18790–18797 (2019).
25. Shimizu, F., Ogata, S. & Li, J. Theory of Shear Banding in Metallic Glasses and Molecular Dynamics Calculations. *Mater. Trans.* **48**, 2923–2927 (2007).
26. Falk, M. L. & Langer, J. S. Dynamics of viscoplastic deformation in amorphous solids. *Phys. Rev. E* **57**, 7192–7205 (1998).
27. Langer, J. S. Shear-transformation-zone theory of plastic deformation near the glass transition. *Phys. Rev. E* **77**, 021502 (2008).
28. Varughese, S., Kiran, M. S. R. N., Ramamurty, U. & Desiraju, G. R. Nanoindentation in Crystal Engineering: Quantifying Mechanical Properties of Molecular Crystals. *Angew. Chem. Int. Ed.* **52**, 2701–2712 (2013).
29. Gurman, S. J. Interpretation of EXAFS Data. *J. Synchrotron Radiat.* **2**, 56–63 (1995).
30. Andrade, F. A., Al-Qureshi, H. A. & Hotza, D. Measuring the plasticity of clays: A review. *Appl. Clay Sci.* **51**, 1–7 (2011).
31. Jung, S., Gwon, H., Yoon, G. & Kim, J. SOLID ELECTROLYTE, METHOD OF PREPARING THE SAME, AND ELECTROCHEMICAL DEVICE INCLUDING THE SAME. *United States Patent US-20210376378-A1* (2021)

32. Kumari, N., Mohan, C., Kumari, N. & Mohan, C. Basics of Clay Minerals and Their Characteristic Properties. in *Clay and Clay Minerals* (IntechOpen, 2021). doi:10.5772/intechopen.97672.
33. Gao, F. Clay/polymer composites: the story. *Mater. Today* **7**, 50–55 (2004).
34. Stoeffler, K., Lafleur, P. G., Perrin-Sarazin, F., Bureau, M. N. & Denault, J. Micro-mechanisms of deformation in polyethylene/clay micro- and nanocomposites. *Compos. Part Appl. Sci. Manuf.* **42**, 916–927 (2011).
35. Jeon, Y. M., Kim, S., Lee, M., Lee, W. B. & Park, J. H. Polymer-Clay Nanocomposite Solid-State Electrolyte with Selective Cation Transport Boosting and Retarded Lithium Dendrite Formation. *Adv. Energy Mater.* **10**, 2003114 (2020).